

Numerical Simulation and Experimental Validation of the Role of Delta Wing Privileged Apex

Iddir Boumrar and Zied Driss

1 Introduction

The designers of the modern aircraft fighters have recently, given unprecedented interest for maneuverability, supersonic cruising, short takeoff, and the landing executions. In particular, supermaneuverability requires significant improvements of the aerodynamic characteristics of the wings at high angles of attack, which initially resulted in seeking geometries of optimal wings allowing and preserving a good dynamics of the turbulent flow at the suction face and eliminating each involved structure in the increase of the aerodynamic drag.

The behavior of the vortex occurring at the delta wing suction face at various incidences has been the subject of research since the beginning of the 50s. The research study developed by Parker (1976) is notable because it contains the complete list of the references and a discussion of the unstable flow for angles of attack going up to 20° .

Many investigators studied the air flow around delta wing models in wind tunnel at subsonic velocities with adapted volatile additives, which gave satisfaction. By employing air, we can reach high Reynolds numbers. For the delta wing model with sharp leading edges, we used Reynolds numbers varying from a few thousands until one or two millions. In a steady flow, when the delta wing incidence increases until a range between 30° and 40° , the exact value depends on the wing aspect ratio and other geometrical parameters; an instability of vortex known under the name of

I. Boumrar (✉)

Laboratory of Energétic Mechanics and Materials—LEMM,

University of Tizi-Ouzou, Tizi Ouzou, Algeria

e-mail: boumrari@hotmail.fr; boumrar_iddir@ummto.dz

Z. Driss

Laboratory of Electromechanical Systems (LASEM), University of Sfax,

Sfax, Tunisia

e-mail: Zied.Driss@enis.tn; Zied_Driss@yahoo.fr

© Springer International Publishing AG, part of Springer Nature 2018

Z. Driss et al. (eds.), *CFD Techniques and Thermo-Mechanics Applications*,

https://doi.org/10.1007/978-3-319-70945-1_7

“the bursting or vortex breakdown” appears at the wing trailing edge and progresses gradually ahead until the wing apex. On the delta wing model, this phenomenon was first observed by Lambourne and Bryer (1962). A study of Hawk et al. (1990) identified “a local angle of movements” around 45° from which the vortex bursting occurs. Ekaterinaris and Schiff (1990) showed that instability can be envisaged successfully (at $\alpha = 32^\circ$ on a delta wing with a sweep angle $\varphi = 75^\circ$) by an exact numerical resolution of the Navier–Stokes equations. These authors also mentioned two classes of vortex bursting known as the “bursting in bubble” and the “bursting in spiral”. The behavior of the bursting is known to play a crucial role in the case of unstable movements. The first “generations” of planes, with delta wings, in the United States: the F-102, B-58, and the experimental bomber Xb-70 were not planned to fly at high angles of attack, they nevertheless drew all benefit from the increase of lift due to the apex vortex. Stability in pitching of the supersonic conveyor Concorde incited the first investigations on instabilities. These studies took place in the United Kingdom and were characterized by the work of Lambourne et al. (1964), which studied the consequences of the fast changes of the incidence angle i , like the oscillating data brought back later in detail by Woodgate and Halliday (1971). Laidlaw and Halfman (1956) have measured the pressures on oscillating models of delta wings with sweep angles $\varphi = 60^\circ$ and 75° , but the amplitudes were small, and then the effect of the vortex was negligible; their objective was to evaluate the linear theory for the wings. However, it has reached incidences close to 90° , HARV used strongly beveled leading edges, and fighters in their preliminary design stage relied on the vortex mode coming from their leading edges (Cummings et al. 1990).

The theories published by Lowson (1963) and Randall (1966) were compared with experimental data. Lowson’s analysis was particularly judged to be a rigorous attempt to adapt the work of Brown and Michael (1955) for oscillating movements. Nevertheless, these authors agree with the conclusions of Parker (1976) admitting that the errors between the experimental and theoretical results are significant adding that the comparisons have only a partial success.

It is not easy to quote all the contributions of those who have explored, through photographic and video techniques, the time dependent of the vortex movements. The principal contributions are given below, as simple lists. The order is not significant and it should be noted that some of the quoted articles also included data of forces or aerodynamic pressures. For example, Wang et al. (2003) have undertaken experiments in a water tunnel with 0.4 m of width, 0.4 m of depth, and 6.0 m of length. The experimental model is a delta wing of sweep angle $\varphi = 65^\circ$; the wing leading edges are beveled. In order to facilitate the experimental observations, the suction face of the delta wing was also divided into five parts along the line of the chord, with radial lines resulting from the apex of the wing with a spacing of 10° . The jet is located at the center of the trailing edge with a rectangular exit nozzle of $2.4 \text{ cm} \times 0.3 \text{ cm}$. The variations of the jet orientation have been achieved by installing various jet openings in the trailing edge of the model. The experiments were considered at Reynolds numbers based on the chord of the wing of about 9.54×10^3 . A dye was injected through 1-mm-diameter openings placed at the

vicinity of the model apex to visualize the vortex bursting. An apparatus was used to record the flow models; the experiments were undertaken in a range of angles of attack $i = 25^\circ\text{--}40^\circ$ with a step of 5° . The exact position of vortex bursting is located at approximately 3–5 mm at the apex. In these experiments, the jet velocity changed from 0 to 10 m/s, and the jet angle from 0° to 60° toward the left side of the model. The motionless photographs show the hysteresis of the wake profiles and the vortex positions, with discussions of the flow details. Lang (2004) designed hypersonic vehicles using the delta wings configuration; ELAC was conceived as a system of transport for future orbital missions. Its first stage is carrying a body, and its second stage is to remain at an orbital altitude of approximately 30 km at $M = 7$. Initially, a combination of the oil flow and a vapor screen was applied to obtain visualizations of vortices at the top of the wing. The visualization of flow and PIV measurements are taken in the transonic wind tunnel with a $40 \times 40\text{-cm}^2$ -sized test section. It is a wind tunnel with intermittent operation, which allows periods of approximately 3 s with Mach numbers of $M = 0.2\text{--}4$. The flow visualization at a relative length of chord $x/l = 30\%$ was carried out on a 1:100 scale model. The flow qualitative research at control faces of the ELAC and PIV measurements was carried out on a 1:240 scale model of a delta wing with sweep angle $\varphi = 75^\circ$, with rounded leading edges to reduce the heat flow at the conditions of hypersonic flight. The Reynolds numbers are about $Re = 3.7 \times 10^6$, with Mach numbers $M = 2.0$ to $M = 2.5$. The experimental techniques applied were also used for the numerical simulation results validation. Many values on the position of the vortex core and its bursting are given.

Brodetsky et al. (2001) developed experiments in a supersonic wind tunnel where a maximum Mach number of 6 was reached. The tests were carried out on three delta wing models with respective sweep angles $\varphi = 68^\circ, 73^\circ, \text{ and } 78^\circ$ and chords 383, 439, and 526 mm, at Mach numbers $M = 2\text{--}4$ and the angles of attack varying from $\alpha = 0^\circ$ to 22° . The testing methods included the measurement of the static pressure on the model face and the flow visualization by the laser sheet technique. Photographs of the laser sheet and oil flow show the evolution of the swirling structure at a fixed angle of attack α . Also, the shock wave positions, size, and the position of primary and secondary vortex were obtained. Some new flow modes around delta wing were identified, and several visualizations were examined. Tests were carried out by Konrath et al. (2008) in a transonic wind tunnel; the test section has a size of $1 \text{ m} \times 1 \text{ m}$ and communicates with a room, in which the total pressure can be placed in one range from 30,000 to 150,000 Pa. The test section was perforated, to give access for small indicators installed on top and on the lower wall behind which cameras, and PSP light sources were placed. The delta wing of sweep angle $\varphi = 65^\circ$ provided by NASA was equipped with beveled and rounded leading edges. First, the PSP method was applied to capture the pressure distributions on the wing suction face; second, the PIV method was used in perpendicular plans to the axis of the model at the positions of chord $x/l = 0.35\text{--}0.9$ for selected angles of attack.

Gursul et al. (2007) studied the concepts of vortex control, which depends on the control of the turbulent flow above the delta wing and enjoys various advantages,

such as the lift improvement, drag reduction, and noise attenuation due to the interaction vortex/wing. The control methods include one or more of the following phenomena: the flow separation around the wing, its reattachment on the wing faces, and the vortex bursting. The flow reattachment on the wing faces moves with the increase of the angle of attack and reaches the wing center line at a particular incidence. In these conditions, this particular incidence decreases with the increase of the apex wing. On thicker wings, the vortex bursting appears at very small incidences. The vortex control methods have become increasingly new and diverse. It is useful to consider the physics of the dominant bursting mechanisms which determine the flow control methods.

The state of the art on the various control solutions suggested in the literature was investigated, in order to determine an adequate solution to the aeronautical problems. In order to achieve the objectives previously mentioned, passive (which do not require an external contribution of energy: like the optimization of the wing form) or active (requiring an external contribution of energy: aspiration and blowing of the boundary layer) solutions can be considered. However, most authors did not take into account the interaction of the wing with the wind tunnel walls. The experimental solutions brought by the authors, in particular the blowing and the aspiration of the boundary layer, are the most encouraging solutions of rupture. They made it possible to delay the apex vortex bursting by delaying the layers separation or aspiring it. Nonetheless, they took into account the induced experimental error and the negative effect which these active systems may have on aerodynamics lift and drag. However, no study reported the drag reduction or lift increase of the delta wing through using the concept of privileged angles, on the delta wing geometry, and therefore a great deal of complementary work is still necessary.

Beyond the visualizations and phenomenological analyses existing in the literature, the study suggested here aimed to be a work of quantification, through the parietal pressure distribution. The principal objective was to dissociate the wings with privileged apex from the wings with non-privileged apex and consequently enable us to choose the delta wings.

A series of pressure taps were placed under the principal apex vortex in order to determine the longitudinal distribution of the defect pressure coefficient $-C_p$; finally, the obtained experimental results were confronted. For the three studied delta wings having the following apex angles ($\beta = 75^\circ$, 80° , and 85°), the results relating the various aerodynamic coefficients show that the wing with privileged apex angle $\beta = 80^\circ$ has the advantage of presenting the greatest depression values, while the two other delta wings with non-privileged apex angles ($\beta = 75^\circ$ and 85°) presented lower depression values.

From these results, it can be concluded that it is preferable to use delta wings with privileged apex angle, which allows us better aerodynamic performances. Comparisons between planes provided with delta wings would prove that the wings with privileged apex have advantages related to the stability of the aircrafts and their fuel consumption.

2 Concept of Privileged Angles

Studies in some interesting fields of science, nature, medicine (physiology, anatomy), architecture, physics, and mechanics are more interested in the phenomenological analyses and tend to generalize the existence of privileged angles. In the aerodynamics field, studies based on many visualizations in wind and hydrodynamic tunnels, of flow around bodies of revolutionized and simple delta wings, show that the angle formed by the apex vortex is affected by the wing apex angle value.

The criterion of privileged angle was highlighted, at the atom microscopic scale, and was found by Leray et al. (1972) to exist at a macroscopic scale in the case of Helium II supra fluid flow between the helicoids swirls and their axis. These privileged angles are given by the same following relation (Leray et al. 1985):

$$\cos \beta_{l,m} = \frac{m}{\sqrt{l(l+1)}}, \tag{1}$$

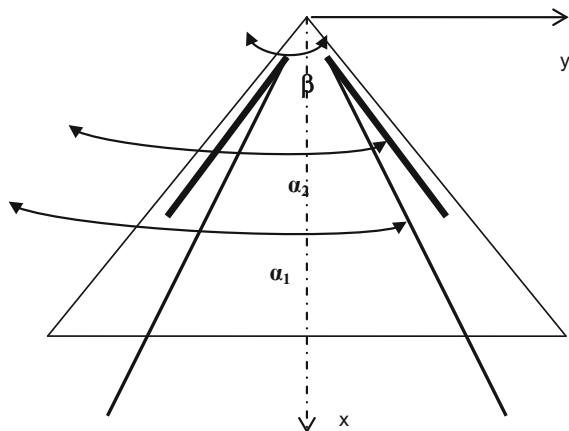
where l and m are integer and with $-l < m < l$.

In Fig. 1, β is the apex angle, α_1 is the angle between the principal vortices, while α_2 is the angle between the secondary vortices.

The above relation (1) enables us to calculate the two main families of privileged angles:

- For $m = l$, we obtain the first family of privileged angles;
- For $(m = 2, l \geq 2)$, we obtain the second family of privileged angles.

Fig. 1 Vortical system on the upper face of non-privileged delta wing



3 Numerical Method

3.1 Boundary Conditions

A three-dimensional flow simulation around the combinations delta wings–fuselage was carried out using the code Fluent 6.1.22 software (2001). The best way of modeling the test conditions in the wind tunnel was to create a square area around the three-dimensional delta wing with a 300 mm of length and a 300 mm of height. For the rectangular sides of left and right of the field, the flow admission was given by “Velocity Inlet” and the type of “Exit” was adopted. The four other sides were considered as walls conditions in the section of the wind tunnel. Calculations were carried out for the flow nominal velocity $V_0 = 20$ m/s.

3.2 Mathematical Formulation

The Spalart–Allmaras turbulence model with one equation was used during simulations. The solution variables of the instantaneous Navier–Stokes equations were decomposed into the mean and fluctuating components (for the velocity: $u_i = \bar{u}_i + u'_i$). Substituting their expressions in the instantaneous continuity and momentum equations, and taking a time average, yields they can be written in Cartesian tensor form as

$$\frac{\partial \rho}{\partial t} + \frac{\partial(\rho u_i)}{\partial x_i} = 0 \quad (2)$$

$$\frac{\partial(\rho u_i)}{\partial t} + \frac{\partial(\rho u_i u_j)}{\partial x_j} = -\frac{\partial p}{\partial x_j} + \frac{\partial}{\partial x_j} \left[\mu \left(\frac{\partial u_i}{\partial x_j} + \frac{\partial u_j}{\partial x_i} - \frac{2}{3} \delta_{ij} \frac{\partial u_i}{\partial x_i} \right) \right] + \frac{\partial}{\partial x_j} \left(-\rho \overline{u'_i u'_j} \right) \quad (3)$$

($i = 1, 2, 3$).

It is worth noting, now, that some additional terms that represent the effects of turbulence appear. These Reynolds stresses, $-\rho \overline{u'_i u'_j}$, must be modeled in order to close Eq. (3). A common method employs the Boussinesq hypothesis to relate the Reynolds stresses to the mean velocity gradients:

$$-\overline{u'_i u'_j} = \frac{\mu_t}{\rho} \left(\frac{\partial u_i}{\partial x_j} + \frac{\partial u_j}{\partial x_i} \right) - \frac{2}{3} \left(k + \frac{\mu_t}{\rho} \frac{\partial u_i}{\partial x_i} \right) \delta_{ij} \quad (4)$$

The Boussinesq hypothesis is used in the Spalart–Allmaras model. The advantage of this approach is the relatively low computational cost associated with the computation of the turbulent viscosity μ_t . In the case of Spalart–Allmaras model,

only one additional transport equation (representing turbulent viscosity) is solved. Note that since the turbulence kinetic energy k is not calculated in the Spalart–Allmaras model, the last term in Eq. (4) is ignored when estimating the Reynolds stresses.

3.3 Grid

The type of grid element employed, schematized on Fig. 2, is triangular. Besides, an unstructured grid was applied. The majority of the significant properties of the flow to be reproduced are in the proximity of the wing surface. Consequently, the

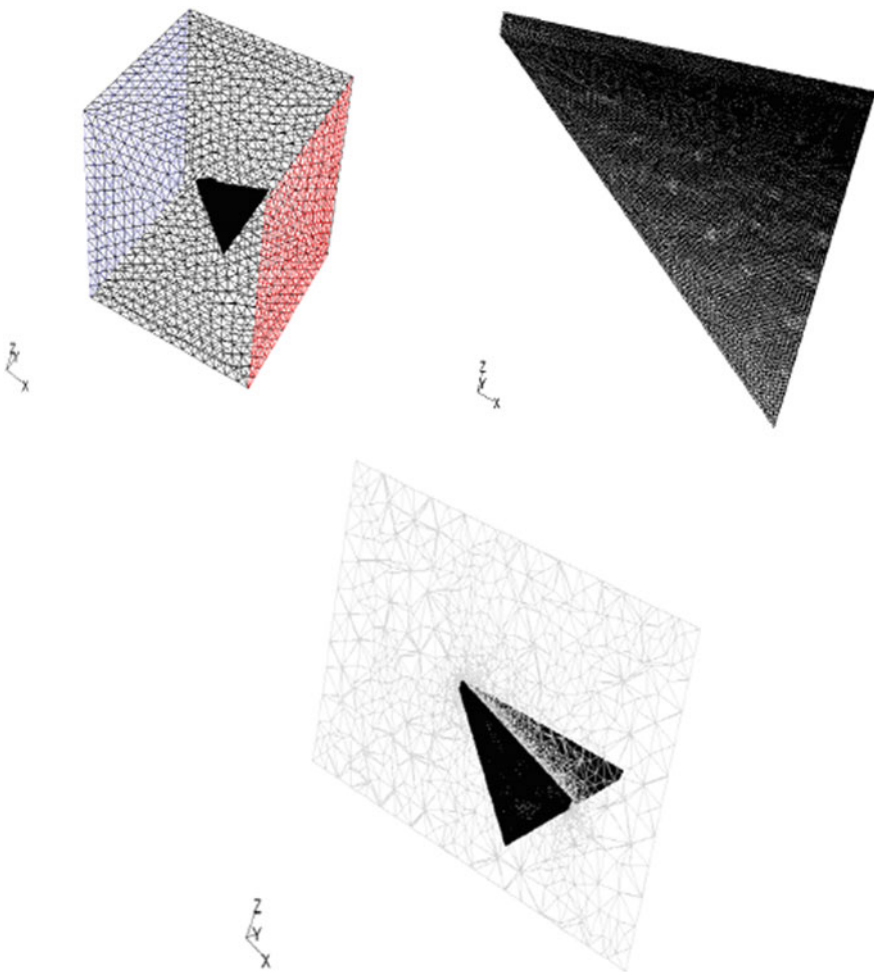


Fig. 2 Meshed geometry example (wing and delta wing–fuselage combination)

meshed field of calculation was refined close to the suction face and the wing faces. However, it was maintained gross in the rest areas of the field to decrease the calculation time.

4 Numerical Results

4.1 Defect Pressure Coefficient $-C_p$ Contours

Figures 3, 4, and 5 present the distribution of the defect pressure coefficient $-C_p$ contours obtained with the numerical simulation, at the suction face of the various studied delta wings. The vortex structure developing at the suction face of the delta wings was reproduced compared to the visualizations results of Benkir (1990).

In Fig. 4, we remark that the angle between the apex vortices direction is very affected by the presence of the fuselage diameter $d = 20$ mm. This fact is valuable for the delta wing with apex angles $\beta = 75^\circ$, 80° , and 85° . The value of $-C_p$ is important for the case of wing without fuselage for all the studied apex.

In Fig. 5, we see that the apex vortices move toward the delta wing leading edges and an interaction zone between the delta wing and the fuselage appeared at the junction point for the two considered fuselages of diameters $d = 20$ mm and $d = 30$ mm.

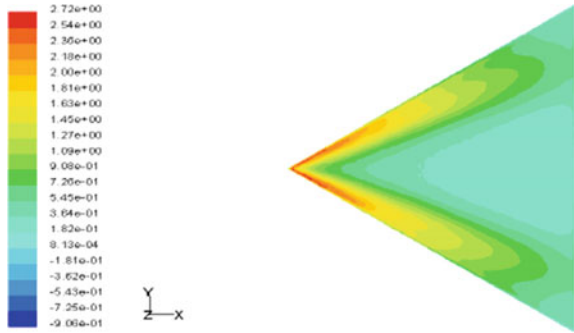
4.2 Transverse Evolution of Defect Pressure Coefficient $-C_p$

Figures 6 and 7 show that according to the four cross sections considered at the top of the delta wings, we note that the apex vortex position is detected by the maximum value of $-C_p$. The maximum value of $-C_p$ decreases when a cylindrical fuselage of diameter d is introduced.

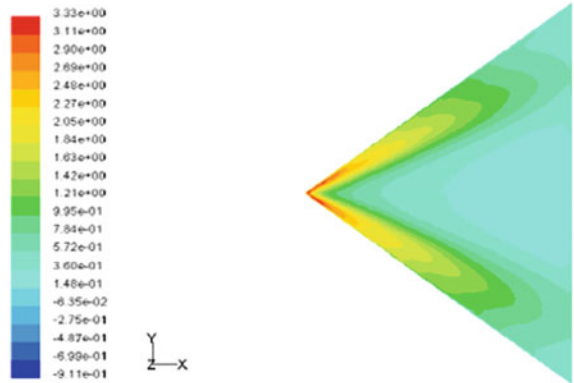
4.3 Role of the Privileged Apex Angle $\beta = 80^\circ$

The longitudinal evolution of the defect pressure coefficient $-C_p$ which is shown in Fig. 8 proves clearly that there is an effect of the privileged angle apex $\beta = 80^\circ$ and the value of the most significant $-C_p$ is reached around $r/l_0 = 0.3$ for the Reynolds number 1.23×10^5 . Through the longitudinal evolution of the defect pressure coefficient $-C_p$, under the principal apex vortex, we can easily notice the maximum

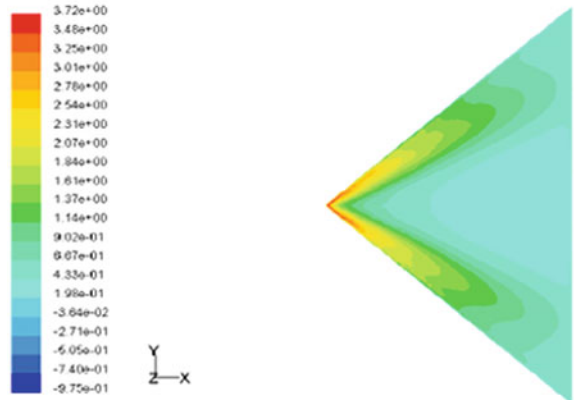
Fig. 3 Contours of $-C_p$ at the suction face of delta wings without fuselage at $V_0 = 20.3$ m/s and an incidence angle $i = 15^\circ$



(a) Apex $\beta = 75^\circ$.

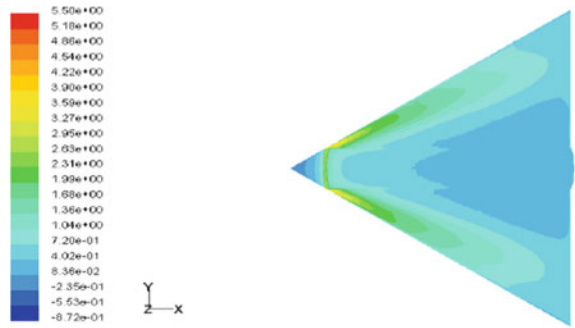


(b) Apex $\beta = 80^\circ$.

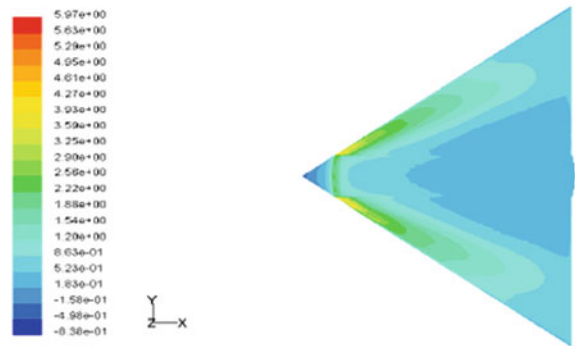


(c) Apex $\beta = 85^\circ$.

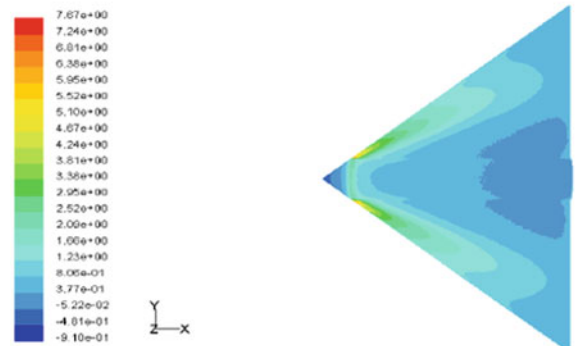
Fig. 4 Contours of $-C_p$ at the suction face of the combinations delta wings-fuselage with a diameter $d = 20$ mm at $V_0 = 20.3$ m/s and an incidence angle $i = 15^\circ$



(a) Apex $\beta = 75^\circ$.

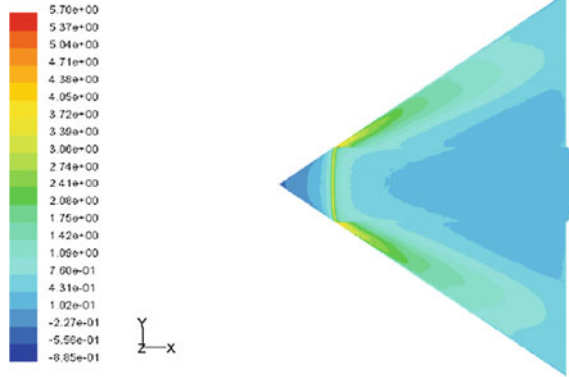


(b) Apex $\beta = 80^\circ$.

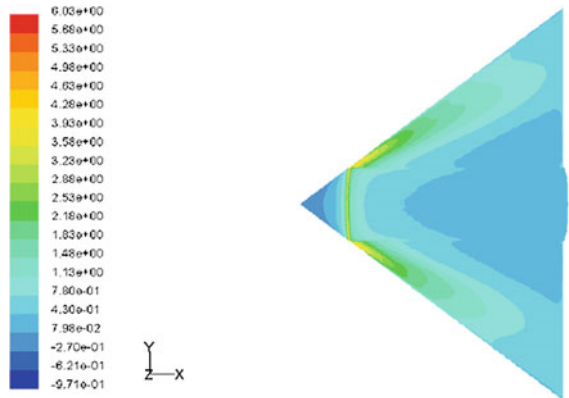


(c) Apex $\beta = 85^\circ$.

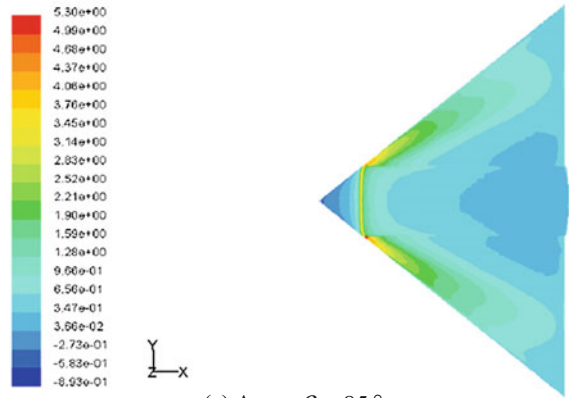
Fig. 5 Contours of $-C_p$ at the suction face of the combinations delta wings-fuselage with a diameter $d = 30$ mm at $V_0 = 20.3$ m/s and an incidence angle $i = 15^\circ$



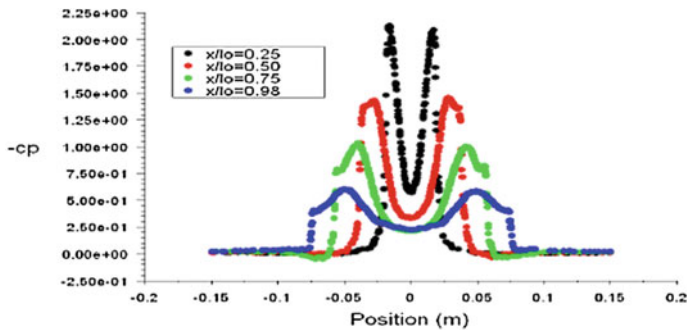
(a) Apex $\beta = 75^\circ$.



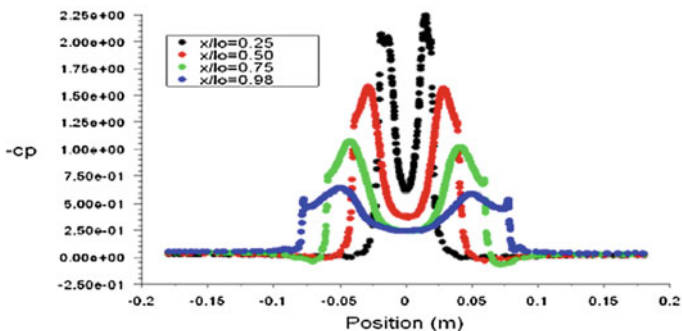
(b) Apex $\beta = 80^\circ$.



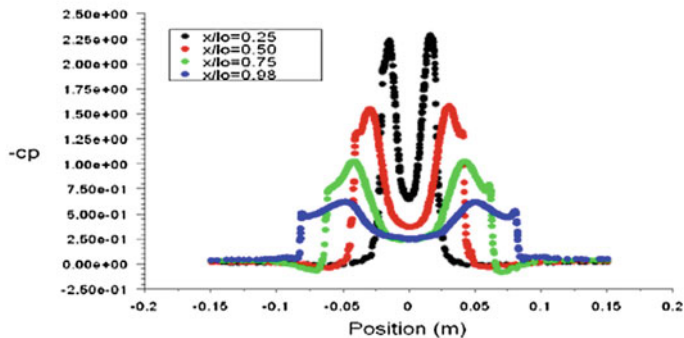
(c) Apex $\beta = 85^\circ$.



(a) Wing with apex angle $\beta=75^\circ$.

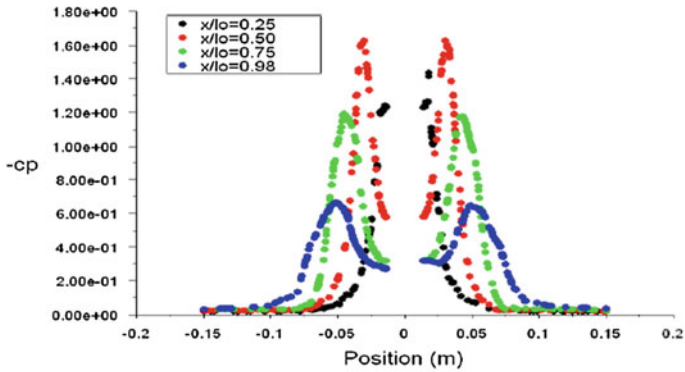


(b) Wing with apex angle $\beta=80^\circ$.

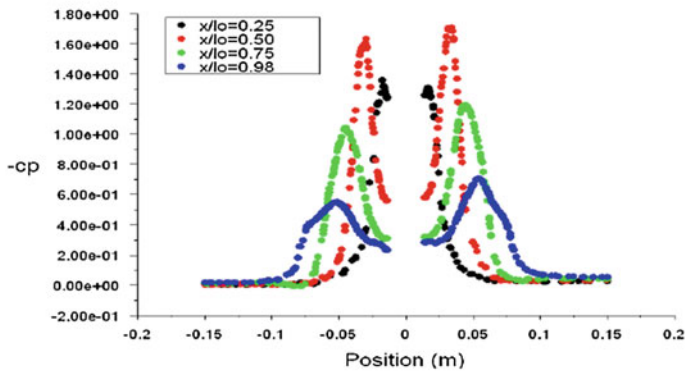


(c) Wing with angle of apex $\beta=85^\circ$.

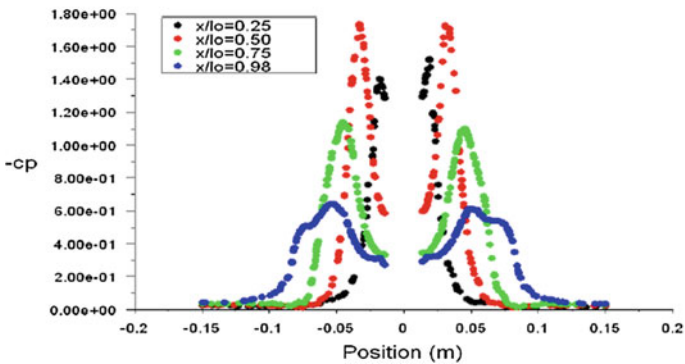
Fig. 6 Transverse evolution of numerical $-C_p$ at the suction face of the delta wings without fuselage at $V_0 = 20.3$ m/s and incidence $i = 15^\circ$



(a) Wing with apex angle $\beta=75^\circ$.



(b) Wing with apex angle $\beta=80^\circ$.



(c) Wing with angle of apex $\beta=85^\circ$.

Fig. 7 Transverse evolution of numerical $-C_p$ at the suction face of the combinations delta wings–fuselage $d = 30$ mm at $V_0 = 20.3$ m/s and an incidence angle $i = 15^\circ$

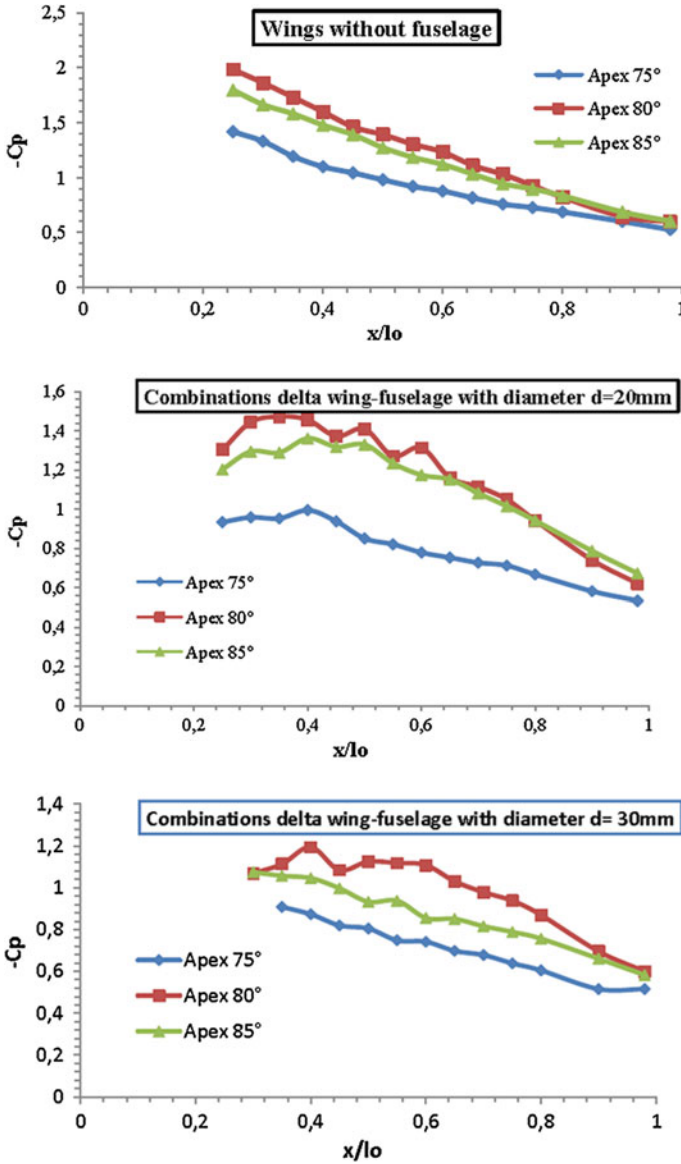


Fig. 8 Longitudinal evolution of the numerical defect pressure coefficient $-C_p$ under the principal apex vortex of delta wings without fuselage and combinations delta wing-fuselage at $V_0 = 20.3$ m/s and an incidence angle $i = 15^\circ$

numerical values of $-C_p$ for the wing with privileged angle apex $\beta = 80^\circ$. This fact is valuable for the wings without fuselage or for the combinations delta wing-fuselage (Fig. 8).

4.4 Fuselage Diameter Effects

Figure 9 shows the effect of the fuselage diameter on the longitudinal evolution of the numerical $-C_p$ under the apex vortex at $V_0 = 20.3$ m/s and an incidence angle $i = 15^\circ$. According to these results, it can be noted that for $x/lo < 0.6$ corresponding to the vicinity immediate of the delta wing apex, the maximum values of $-C_p$ are obtained with the wing without fuselage. Then, the values corresponding to the combination delta wings–fuselage appear with diameter $d = 20$ mm and lastly those corresponding to the combination with $d = 30$ mm. Beyond $x/lo = 0.60$, i.e., when we move toward the wing trailing edge, the same order is preserved with a tendency of confusion of the considered curves (Fig. 9).

According to these results, we can deduce that we have the same evolution of the numerical results concerning the role of privileged apex angle $\beta = 80^\circ$ (Fig. 8) for the wings without fuselage and for the combinations delta wing–fuselage. The effect of the diameter presence is the same concerning the three studied apex cases (Fig. 9).

5 Comparison with Experimental Results

The current way used to ensure the quality of the numerical simulations is the calculation of the aerodynamic characteristics such as pressure distribution and forces, and compares them with the experimental results obtained in the wind tunnel.

The numerical and the experimental results are confronted in the same graphs (Figs. 10 and 11) for better elucidating the difference. According to these figures, it was noted that for the wings without fuselage, the defect pressure coefficient read on the experimental and numerical curves are in good agreement, and the difference between these two last curves is due to the resolution of the Navier–Stokes equations with simplifying assumptions. For the case of the combination delta wing–fuselage, the difference between the experimental and the numerical curves increases as we approach the wing apex.

For the combinations wing–fuselage (Fig. 11), the two curves converge when we move away from the apex of the wing. In fact, the difference between the two curves is more significant at the vicinity of the apex and becomes negligible when we approach the trailing edge of the wing.

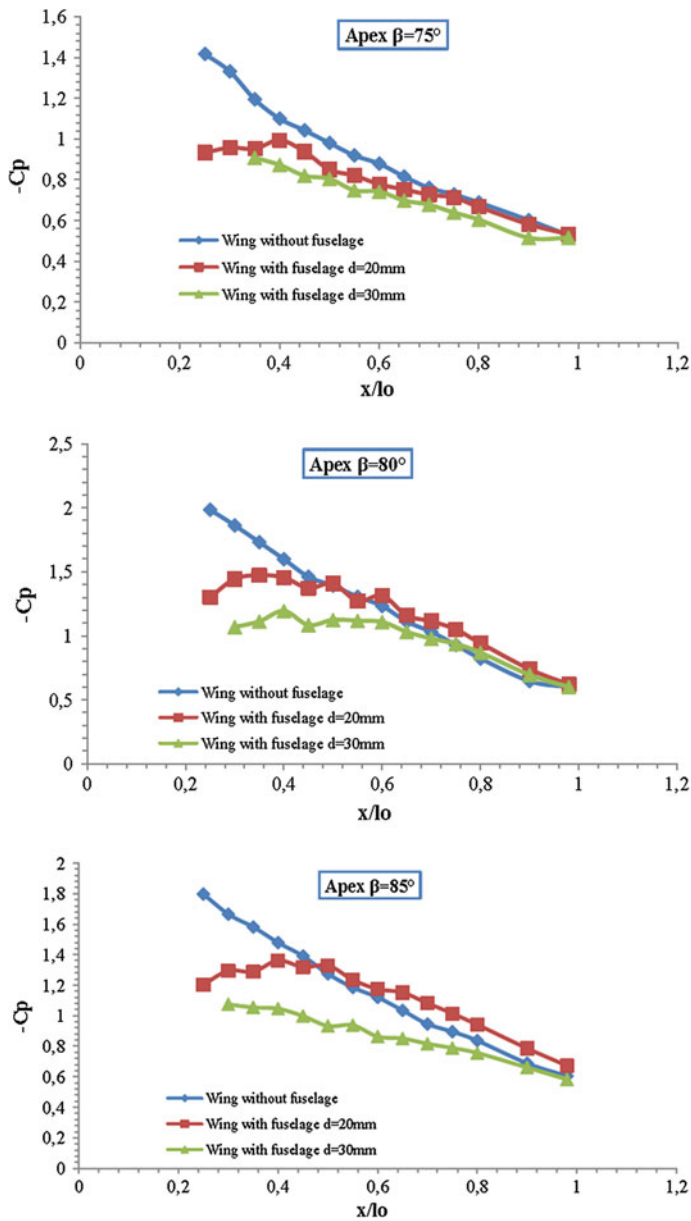


Fig. 9 Fuselage diameter effect on the longitudinal evolution of the numerical $-C_p$ under the apex vortex at $V_0 = 20.3$ m/s and an incidence angle $i = 15^\circ$

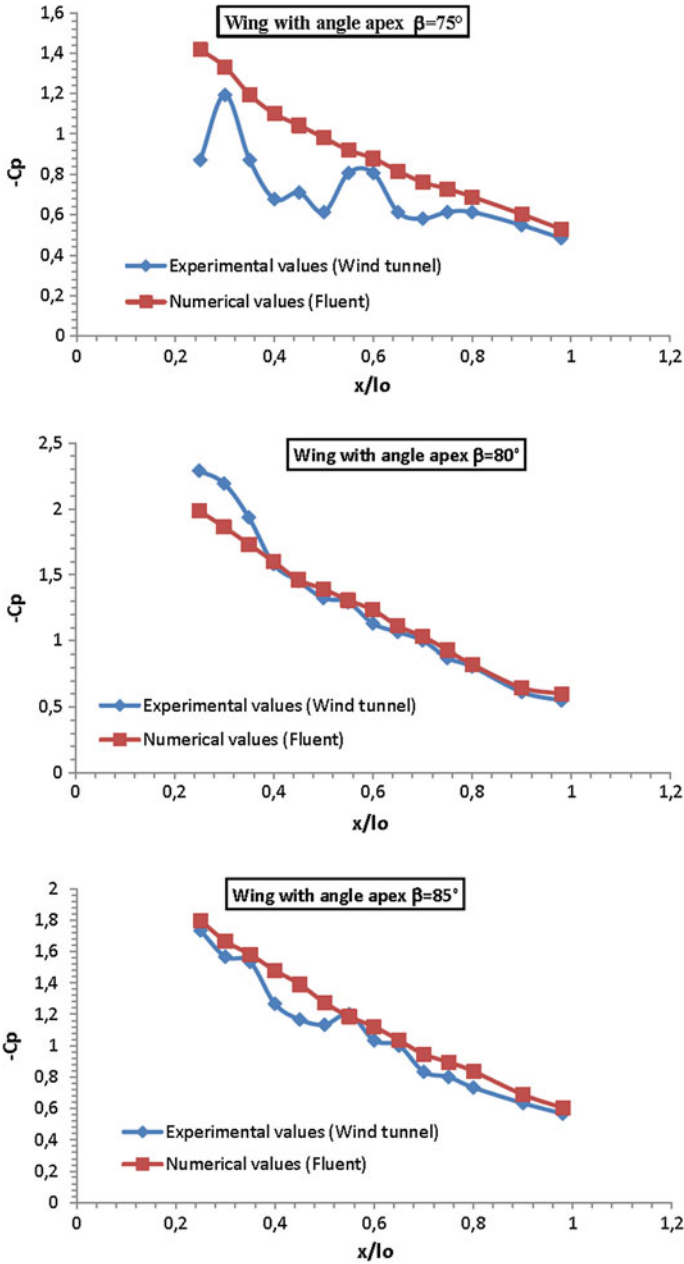


Fig. 10 Comparison between the numerical and experimental values of $-C_p$, under the principal apex vortex, for the delta wings without fuselage at $V_0 = 20.3$ m/s and an incidence angle $i = 15^\circ$

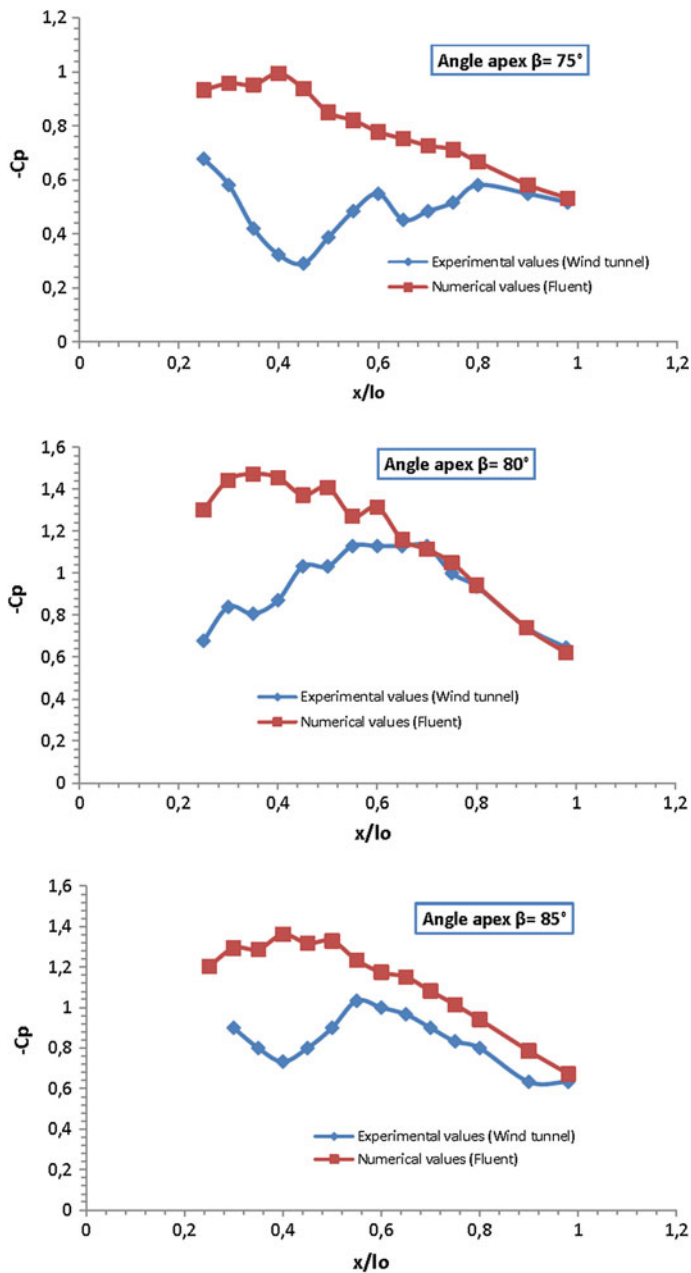


Fig. 11 Comparison between the numerical and experimental values of $-C_p$, under the principal apex vortex, for the various combinations delta wing-fuselage with diameter $d = 20$ mm at $V_0 = 20.3$ m/s and an incidence angle $i = 15^\circ$

6 Conclusions

The discussions of the various experimental and numerical results were achieved by taking into account the geometrical and kinematics parameters, and we can, thus, conclude that

- (1) the increase of the incidence always generates an increase in the coefficient of depression $-C_p$, for all the studied wings as long as the incidence of the wing is lower than the critical incidence (incidence of vortex bursting).
- (2) at the high attack angles ($i > 25^\circ$), the flow at the extrados of the delta wings without fuselage was mainly asymmetrical, and the part close to the apex shows high values of $-C_p$. The effects of the Reynolds number on the flow around the delta wings without fuselage are not significant. The vortex breakdown incidence of the apex vortex is reached at lower incidences for the wings with apex angles $\beta = 80^\circ$ and 85° ($i_{vb} = 22^\circ\text{--}25^\circ$), compared to the wing with angle apex $\beta = 75^\circ$ ($i_{vb} = 30^\circ$). This fact is valid for the all used velocities flow.
- (3) the depression values corresponding to the delta wings with privileged apex angles are more significant than those obtained for the wings with non-privileged apex angles $\beta = 75^\circ$ and 85° , which enables us to reach one of the objectives fixed at the beginning of our work consisting on studying the role of the privileged angle on flow around delta wings.

A systematic experimental study was carried out for three configurations of delta wing–fuselage at various attack angles and flow velocities. We observe, on the combinations delta wing–fuselage, the effects of the privileged angle $\beta = 80^\circ$ until the attack angle $i = 22^\circ\text{--}25^\circ$, where the apex vortex breakdown takes place, downstream from $r/l_0 = 0.6$; a slight change of flow was recorded through the aerodynamic characteristics evolution.

At high attack angles ($i > 25^\circ$), the flow around the combinations delta wing–fuselage was mainly asymmetrical, and the fuselage induces the asymmetry of vortex or its bursting or both. The effects of the Reynolds number on the flow around the combination delta wing–fuselage are insignificant.

Comparing the numerical and experimental results, we have noticed a better reproduction of the apex vortices at the suction face of the studied delta wings and a very good agreement between these results for the studied wings and combination delta wings–fuselage.

Simulation of airflow around the delta wing and around the various studied combinations enabled us to well understand the physical phenomenon through the obtained contours of defect pressure coefficient and velocity.

In addition, by analyzing the flow around the various combinations, it has been noted that the role of the privileged angle apex $\beta = 80^\circ$ appears for the delta wings without fuselage and with fuselage of diameters $d = 20$ mm and $d = 30$ mm.

So far, the obtained numerical results have evolved in the good direction: no contradictions were remarked between the achieved simulations and the measurements really undertaken in the wind tunnel.

Nomenclature

C_p	Pressure coefficient
g	Acceleration of gravity
i	Angle of attack (AOA $^\circ$): incidence ($^\circ$)
i_{cr}	Critical incidence ($^\circ$)
i_{vb}	Vortex breakdown incidence ($^\circ$)
k	Kinetic energy
l_o	Wing chord (m)
L	Wing span (m)
O^{xyz}	Cartesian coordinates axis
O^x	Median axis on the wing surface
O^y	Transverse axis on the wing surface
O^z	Vertical axis
r	Polar coordinate of the pressure taps (m),
S	Wing surface (m 2),
u_i	Velocity component (m/s), ($i = 1, 2, 3$),
\bar{u}_i	Mean velocity component,
u'_i	Fluctuating velocity component,
V_0	Wind tunnel velocity (m/s).

Greek Letters

ρ	Air density (kg/m 3),
ρ_H	Oil density (kg/m 3),
α_1	Angle between the principal vortices directions ($^\circ$),
α_2	Angle between the secondary vortices directions ($^\circ$),
β	Apex angle ($^\circ$),
δ_{ij}	Index of Kronecker,
μ_t	Turbulent viscosity (Ns/m 2),
$\lambda = \frac{L^2}{S} = 4tg\left(\frac{\beta}{2}\right)$	Aspect ratio,
θ	Polar coordinate of the pressure taps ($^\circ$),
φ	Sweep angle ($^\circ$).

References

- Benkir M (1990) Persistence et destruction des structures tourbillonnaires concentrées en particulier au dessus d'ailes delta: Critères angulaires de stabilité aux écoulements. Université de Valenciennes, Thèse de Doctorat
- Brodetsky MD, Krause E, Nikiforov SB, Pavlov AA, Kharitonov AM, Shevchenko AM (2001) Evolution of vortex structures on the leeward side of a delta wing. J App Mech Tech Phy 42(2): 243–254
- Brown CE, Michael WH (1955) On slender delta wings with leading-edge separation. NACA Technical note 3430

- Cummings RM, Rizk YM, Schiff LB, Chaderjian NM (1990) Navier-Stokes predictions of the flow field around the F-18 (HARV) wing and fuselage at large incidence. AIAA 90-0099, presented at 28th aerospace sciences meeting, Reno, NV, USA
- Ekaterinaris JA, Schiff LB (1990) Vortical flows over delta wings and numerical prediction of vortex breakdown. AIAA-90-0102, presented at 28th aerospace sciences meeting, Reno, NV, USA
- Gursul I, Vardaki E, Margaris P, Wang Z (2007) Control of wing vortices. In: King R (ed) Active flow control, NNFM 95. Springer, Berlin, pp 137–151
- Hawk JD, Barnet RM, O'neil PJ (1990) Investigation of high angle of attack vortical flow over delta wings, AIAA-90-0101. Presented at 28th aerospace sciences meeting, Reno, NV, USA
- Konrath R, Klein C, Schroder A, Kompenhans J (2008) Combined application of pressure sensitive paint and particle image velocimetry to the flow above a delta wing. *Exp Fluids* 44:357–366 (Research Article)
- Laidlaw WR, Halfman RL (1956) Experimental pressure distributions on oscillating low aspect ratio wings. *J Aeronaut Sci* 23:117–124
- Lambourne NC, Bryer DW (1962) The bursting of leading-edge vortices—some observations and discussion of the phenomenon. Aeronautical Research Council, R&M, No. 3282
- Lambourne NC, Bryer DW, Maybrey JFM (1964) The behavior of leading edge vortices over a delta wing following a sudden change of incidence. Reports & Memoranda No. 3645, Aeronautical Research Council, London, UK
- Lang N (2004) Investigation of the supersonic flow field around a delta wing using particle-image-velocimetry. Aerodynamisches Institut, RWTH-Aachen, Wüllnerstr. zw. 5 u. 7, D-52062 Aachen, Germany
- Leray M, Deroyon MJ, Francois M, Vidal F (1972) New results on the vortex lattice. Proceedings of the 13th international conference on low temperature, Physics LT 13 Boulder, Colorado, USA
- Leray M, Deroyon JP, Deroyon MJ, Minair C (1985) Critères angulaires de stabilité d'un tourbillon hélicoïdal ou d'un couple de tourbillons rectilignes, rôle des angles privilégiés dans l'optimisation des ailes, voiles, coques des avions et navires. Association technique maritime et aéronautique, France
- Lowson MV (1963) The separated flow on slender wings in unsteady motion. Reports & Memoranda No. 3448, Aeronautical Research Council, London, UK
- Parker AG (1976) Aerodynamic characteristics of slender wings with sharp leading edges—a review. *J Aircr* 13(3):161–168
- Randall DG (1966) Oscillating slender wings with leading-edge separation. *Aeronaut Q* XVII:311–331
- User Manual Fluent 6.1.22 (2001) Fluent Inc.
- Wang JJ, Li QS, Liu JY (2003) Effects of a vectored trailing edge jet on delta wing vortex breakdown. *Exp Fluids* 34:651–654
- Woodgate L, Halliday AS (1971) Measurements of the oscillatory pitching-moment derivatives on a series of three delta wings in incompressible flow. Reports & Memoranda No. 3628, parts 1–4, Aeronautical Research Council, London, UK